

Unraveling the Stability of Layered Intercalation Compounds through First-Principles Calculations: Establishing a Linear Free Energy Relationship with Aqueous Ions

Naoto Kawaguchi,* Kiyou Shibata, and Teruyasu Mizoguchi*



Cite This: *ACS Phys. Chem Au* 2024, 4, 281–291



Read Online

ACCESS |

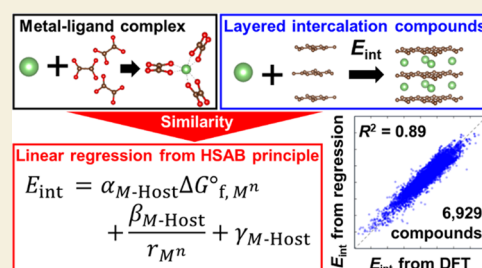
Metrics & More

Article Recommendations

Supporting Information

ABSTRACT: Layered intercalation compounds, where atoms or molecules (intercalants) are inserted into layered materials (hosts), hold great potential for diverse applications. However, the lack of a systematic understanding of stable host–intercalant combinations poses challenges in materials design due to the vast combinatorial space. In this study, we performed first-principles calculations on 9024 compounds, unveiling a novel linear regression equation based on the principle of hard and soft acids and bases. This equation, incorporating the intercalant ion formation energy and ionic radius, quantitatively reveals the stability factors. Additionally, employing machine learning, we predicted regression coefficients from host properties, offering a comprehensive understanding and a predictive model for estimating the intercalation energy. Our work provides valuable insights into the energetics of layered intercalation compounds, facilitating targeted materials design.

KEYWORDS: *first-principles calculation, intercalation, layered intercalation compounds, principle of hard and soft acids and bases, stability*



1. INTRODUCTION

Layered intercalation compounds, which have a structure in which atoms or molecules (intercalants) are inserted into layered compounds (hosts), have been extensively studied because of their characteristic physical properties and the wide variety of synthetic methods available. Due to their ability to intercalate/deintercalate ions and molecules,^{1,2} they are being investigated for applications in energy storage, and various properties resulting from their two-dimensional nature, such as superconductivity,^{3–5} spin glass,⁶ and topological electronic states,⁷ have also been studied. Other novel phenomena have also been reported, such as the change in host electrowetting response⁸ and manipulation of magnetism⁹ due to molecule intercalation. As for synthesis methods, in addition to the general solid-phase, vapor-phase, ion-exchange, and electrochemical insertion methods, a wide variety of synthetic techniques such as zerovalent metal intercalation,¹⁰ liquid alloy,¹¹ molten salt,¹² molecular beam epitaxy, and chemical vapor deposition methods¹³ have been studied in recent years, and various new materials have been synthesized. However, there is no systematic understanding of which combinations of hosts and intercalants are stable, and thus, it is not straightforward to search for new layered intercalation compounds from a vast number of combinations.

In recent years, comprehensive first-principles calculations have been performed in the field of computational science to search for substances in inorganic compounds,¹⁴ and attempts to synthesize substances considered stable from these

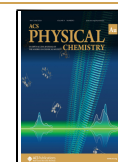
calculations have been widely conducted in various fields, such as cathode materials for Li-ion secondary batteries,¹⁵ solid electrolytes for all-solid-state Li-ion secondary batteries,¹⁶ and semiconductors.¹⁷ Furthermore, databases of materials including virtual structures constructed by first-principles calculations based on density functional theory (DFT),^{18,19} such as the Materials Project²⁰ and the Open Quantum Materials Database,^{21,22} cover the formation energy, E_f , an indicator of stability. The stability of materials with various structures is now widely discussed. These databases have also been used to develop various materials.^{23,24} In addition, there are databases specialized for specific structures, such as 2D materials^{25–27} and perovskites,²⁸ and a data infrastructure called NOMAD,²⁹ where materials databases can be easily uploaded by users. Thus, it can be said that data-driven material development using databases is very active. As software for DFT calculations, there are various codes such as CASTEP,³⁰ the Vienna Ab initio Simulation Package (VASP),^{31–35} and Quantum ESPRESSO.^{36,37} Among them, the VASP code is one of the most widely used simulation codes to build the

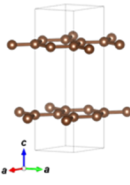
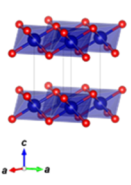
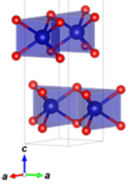
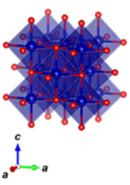
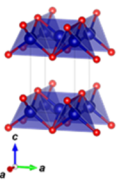
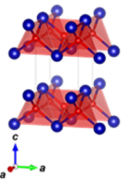
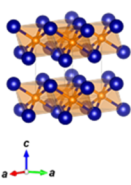
Received: November 23, 2023

Revised: February 8, 2024

Accepted: February 8, 2024

Published: March 7, 2024



Composition	C		AX ₂		A ₂ X ₂		A ₂ Z
Crystal Structure	(a) 	(b) 	(c) 	(d) 	(e) 	(f) 	(g) 
Space Group	<i>P6₃/mmc</i>	<i>P3̄m1</i>	<i>P6₃/mmc</i>	<i>Fm3̄m</i>	<i>P4/nmm</i>	<i>P4/nmm</i>	<i>P3̄m1</i>
Structure Type	Graphite	Octahedral	Trigonal Prism	Rock Salt	Anti-PbO	PbO	Octahedral

A: all elements without lanthanoids and actinoids, X: elements in groups 13 to 17, Z: C or N

Figure 1. Crystal structures and compositions treated as hosts in this study visualized by VESTA.⁵¹

databases due to its versatility and high computational reliability.

In addition, the use of machine learning has been investigated to search for stable new materials, and there have been many attempts to predict the stability of inorganic compounds using new descriptors such as the Coulomb matrix³⁸ and the orbital-field matrix.^{39,40} However, these simulations and predictions are, in many cases, difficult to handle in a generic and quantitative manner to determine what is contributing to the stability of a compound. Similarly, the importance of computational stability discussions has been recognized in layered intercalation compounds as well,⁴¹ and while there have been searches limited to specific hosts, such as the self-intercalation from calculations in transition metal dichalcogenides (TMDs)⁴² and the search for stable graphite intercalation compounds (GICs) we reported,⁴³ universal factors for the stable host–guest combinations have yet to be extracted.

As a new perspective for the stability of the layered intercalation compounds, we focused on the principle of hard and soft acids and bases (HSAB),^{44,45} which is primarily used in complex chemistry to explain that hard acids tend to form ionic bonds with hard bases, while soft acids tend to form covalent bonds with soft bases due to the spread of electron clouds. The HSAB principle has been widely employed in complex chemistry to understand the stable ligand–central atom combinations, and various quantitative indices have been proposed, such as the chemical softness (η) introduced by Parr and Pearson.⁴⁶ There are few reports where the HSAB principle has been used for understanding crystalline systems. For example, in binary ionic crystalline materials, the value of η calculated from two elements and the sum of their ionic radius have been utilized to quantitatively evaluate lattice energy.⁴⁷ However, this idea is applicable only to the binary materials, and most research of the stability quantification using the HSAB principle is limited to the complexes. Nevertheless, considering the intercalant as the complex center and the host as the ligand, the relationship between the two is similar, and the importance of a covalent electron density distribution around the intercalant has been emphasized through the systematic simulation of GICs.^{48,49} Thus, we believe that the concept of the HSAB principle could be applicable to understanding the stability of layered intercalation compounds as well.

Based on the background described above, in this study, we conducted systematic first-principles calculations on various

layered intercalation compounds with different intercalants to calculate their structures and energies, creating a database. While databases specialized for layered structures, such as 2D materials, exist,^{25–27} this study is the first to establish a database specifically for the layered intercalation compounds. Notably, our database is distinctive not only in its coverage of stable compounds with high synthesizability but also in its comprehensive calculation of less stable compounds. This approach allows for a thorough examination of the underlying physics, facilitating discussions on factors influencing both stability and instability. Next, we attempted to identify the factors contributing to the stability of layered intercalation compounds from the perspective of the HSAB principle. As a result, we discovered that the intercalation energy required for intercalation of layered intercalation compounds, obtained through the first-principles calculations, can be linearly regressed from the following two physical properties: (1) the standard Gibbs free energy of formation of the intercalant ion and (2) the ionic radius of the intercalant. This relationship is captured by a simple regression equation derived from the HSAB principle. Through this study, we have successfully extracted fundamental principles that provide valuable guidance for the efficient design of layered intercalation compounds within a vast combinatorial space. Our findings suggest potential advancements in diverse applications, and we anticipate the possibility of synthesizing new layered intercalation compounds based on this model.

2. METHODOLOGY

2.1. Preparation of Crystal Structures of Layered Intercalation Compounds

Seven types of structures and compositions were selected as hosts, C, AX₂, A₂X₂, and A₂Z, and their crystal structures are shown in Figure 1, where A represents all elements except lanthanides and actinides, X represents elements in groups 13–17, and Z represents C or N. In order to perform accurate regression, stable convergence of energy and structure calculations is required for various layered intercalation compounds. However, the interlayer compounds containing lanthanides and actinides have poor convergence in the calculations and are an obstacle to creating a high-quality database; thus, they had to be excluded in this study. Figure 1 (a) shows graphite, the host of typical layered intercalation compounds, GICs, and the five crystal structures of GICs experimentally reported to date are shown in Figure S1. Figure

1 (b) and (c) shows the structures with the composition AX_2 , with an octahedral structure and a triangular prismatic structure, respectively. Figure 1(d–f) represents structures with the composition A_2X_2 (relative to the composition of the intercalant, one). Figure 1(d–f) shows rock-salt, anti-PbO, and PbO structures, respectively. The difference between Figure 1(e,f) is whether the outer layer of the two constituent elements is anionic or cationic, and in this study, the distinction is made by the electronegativity (Allred-Rochow's scale)⁵⁰ of the two elements. Figure S4 shows the crystal structures of these host compounds. Figure 1(g) shows a layered material with the composition ZA_2 ($Z = C, N$) with an octahedral structure. This crystal structure can be regarded as a termination-free structure of a substance called MXene. The intercalated crystal structures of this host are shown in Figure S5, which is known as the MAX phase.

As intercalants, the elements colored in Figure 2 were selected. These elements were chosen based on the availability

H																				He
Li	Be									B	C	N	O	F	Ne					
Na	Mg									Al	Si	P	S	Cl	Ar					
K	Ca	Sc	Ti	V	Cr	Mn	Fe	Co	Ni	Cu	Zn	Ga	Ge	As	Se	Br	Kr			
Rb	Sr	Y	Zr	Nb	Mo	Tc	Ru	Rh	Pd	Ag	Cd	In	Sn	Sb	Te	I	Xe			
Cs	Ba	<i>Ln</i>	Hf	Ta	W	Re	Os	Ir	Pt	Au	Hg	Tl	Pb	Bi	Po	At	Rn			
Fr	Ra	<i>Ac</i>																		

Figure 2. Elements were treated as intercalants. The elements represented in blue become cations, while those represented in red become anions when they are hydrated.

of standard Gibbs free energy of ion formation and effective ionic radius data extracted from the references,^{52–56} excluding lanthanides and actinides for the same reason mentioned above. Elements in blue are more likely to become cations when hydrated, while those in red are more likely to become anions.

The crystal structures of the layered intercalation compounds were created based on these structures and elements. The method is shown in Figure 3. For substances other than GICs, compounds with the crystal structures shown in Figures S2–S5 were screened by the compositional formula and space group from the Materials Project,²⁰ a comprehensive database of inorganic compounds. Subsequently, only substances that had been reported experimentally were extracted and substances with the same host and stacking were excluded. Subsequently, intercalants M were removed from the structures of the layered intercalation compounds, and the layered compound structures shown in Figure 1 were created as hosts. Then, first-principles calculations were performed on the hosts, and those structures that could keep layered structures were adopted as hosts, and only the layered intercalation compounds with these hosts were extracted. Note that the layered compounds obtained here as hosts include virtual compounds. For the GICs, we selected the five structures reported in Figure S1, yielding a total of 188 layered intercalation compounds, and by changing the intercalant to the 48 elements shown in Figure 2, we created 9024 structures of layered intercalation compounds. Thus, from a practical perspective, the structures were created by varying the intercalant using layered intercalation compounds with well-known host structures that have been experimentally reported as the parent materials.

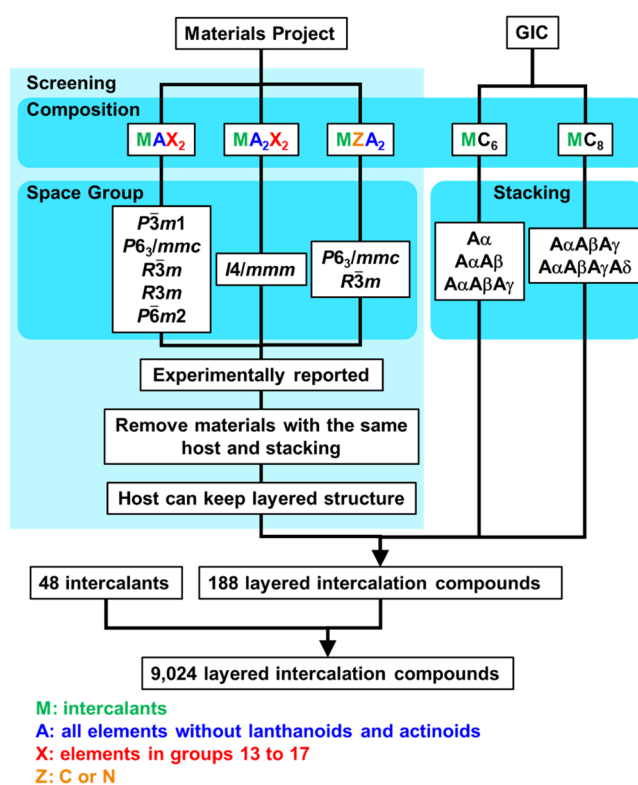


Figure 3. Flowchart of making layered intercalation compounds.

2.2. First-Principles Calculations

First-principles calculations were performed on the obtained layered intercalation compounds and host-only structures. Structural relaxations through simulations based on DFT^{18,19} were performed on the initial structures using the plane-wave basis projector augmented wave method⁵⁷ implemented in the VASP code.^{31–35} For the simulation of the layered compounds, van der Waals dispersion (vdW) forces have to be implemented in the simulation.⁵⁸ To consider the vdW interaction, we systematically tested various vdW density functional methods^{59–63} for the GICs as the reference, confirming the reproducibility of crystal structures and the validity of the formation energies. The results are listed in Table S1. Consequently, we selected the rev-vdW-DF2 method proposed by Hamada,⁶² which was implemented using the algorithm of Román-Pérez and Soler⁶⁴ because both errors were the lowest.

Spin-polarized calculations were performed, but the spin-orbit interaction was not considered. For primitive cell calculations, the Brillouin zone was sampled by odd-number k-point meshes with spacing less than 0.25 \AA^{-1} , using the Monkhorst–Pack scheme.⁶⁵ The electron wave functions were expanded in plane waves up to a kinetic energy cutoff of 650 eV, and the self-consistent field convergence energy was set to 10^{-4} eV. Full structural relaxations of the cell volume and atomic positions were performed until the residual forces on the ions converged to below 0.05 eV/\AA . Subsequently, the cell volume and atomic positions were fixed, and the total energies were calculated using the tetrahedron method with Blöchl corrections.⁶⁶ This computation condition is considered to be accurate enough for all materials in this study for discussing the stability of layered intercalation compounds.

Although the convergence energy of the self-consistent field (10^{-4} eV) is not very strict, we adopted this value to converge

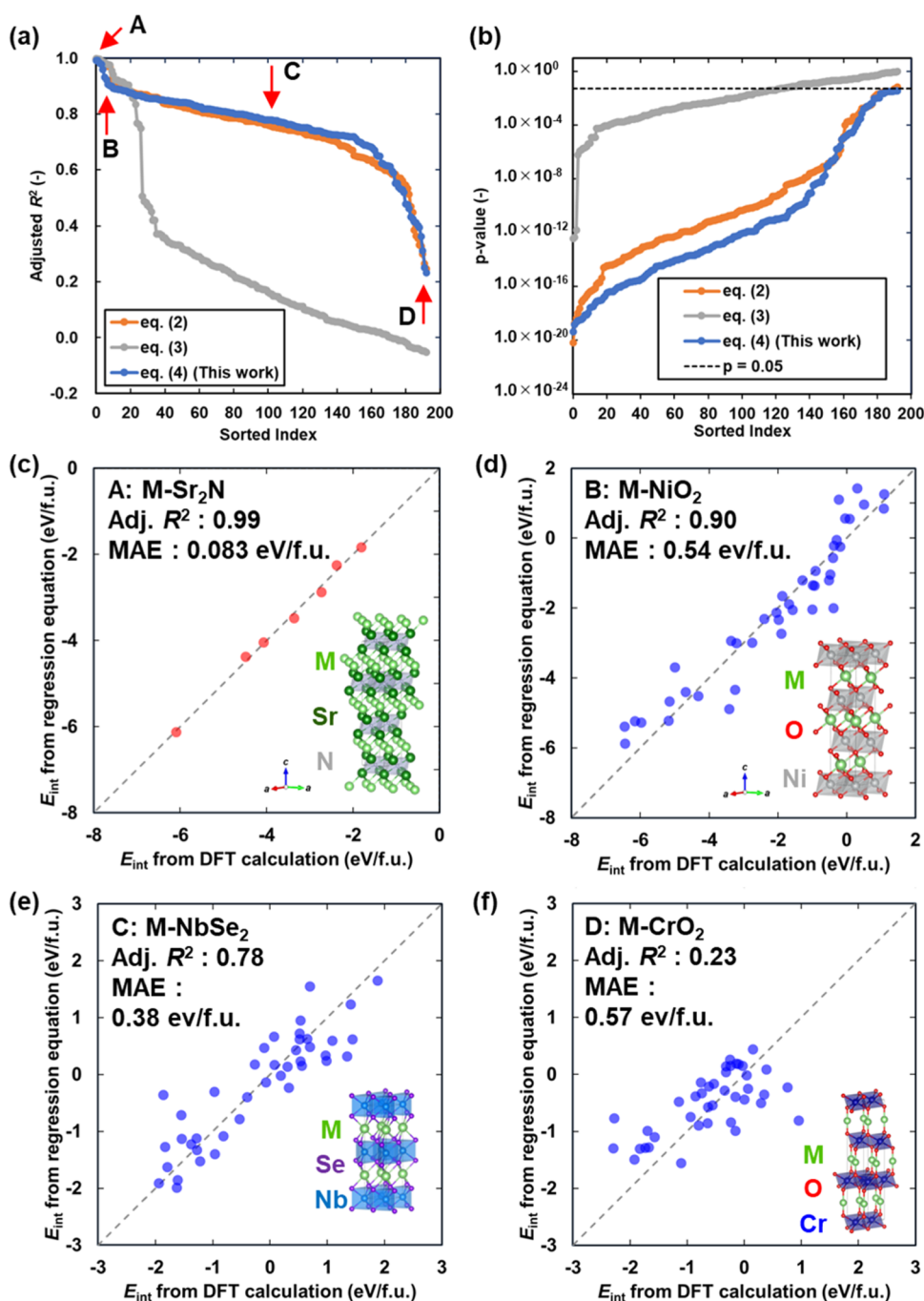


Figure 4. Sorted values of (a) Adj. R^2 and (b) p -values in the F-statistic test in each regression model and examples of regression results of (c) highest Adj. R^2 , (d) highest Adj. R^2 in the base-like host, (e) moderately Adj. R^2 , and (f) lowest Adj. R^2 among eq 4 regressions.

the calculation in a realistic time for creating an exhaustive database. To confirm the accuracy of the present simulation, we performed additional calculations for M-NiO₂ (O4 structure in Figure S2) and M-NbSe₂ (T4 structure in Figure S3) with convergence energies set to 10⁻⁶ eV (namely 2 orders of magnitude stricter than the normal condition) and compared the results, as shown in Figure S6. Based on the fact that there was no significant difference in the total energies, it can be concluded that the present condition is accurate enough for the present study.

2.3. Estimation of Intercalation Energy

The intercalation energy E_{int} was calculated as the energy required for intercalation using eq 1

$$E_{\text{int}} = E_{\text{tot}}(\text{M} - \text{Host}) - E_{\text{tot}}(\text{M}) - E_{\text{tot}}(\text{Host}) \quad (1)$$

where $E_{\text{tot}}(\text{M} - \text{Host})$, $E_{\text{tot}}(\text{M})$, and $E_{\text{tot}}(\text{Host})$ are the calculated total energies of the layered intercalation compound, the standard state of the intercalant, and the host, respectively. The unit of E_{int} is eV/formula unit (f.u.). E_{int} can be interpreted as the reaction energy between the intercalant and host, allowing for a discussion of the stability of the interlayer compound. While a negative value of E_{int} does not imply that the reaction proceeds because the host is often a virtual structure, all hosts in our constructed database have been experimentally reported as a part of stable layered intercalation compounds with one or more intercalants.

Therefore, if their E_{int} values are lower than those of the experimentally reported compounds, they could potentially be synthesized through topochemical reactions such as ion exchange. Essentially, E_{int} enables a discussion of the relative stability of various interlayer compounds from different host and intercalant combinations.

This calculation also allows for the determination of the average voltage associated with intercalation,⁶⁷ which is crucial for energy material applications. Additionally, by replacing $E_{\text{tot}}(\text{Host})$ with $\sum E_{\text{tot}}(\text{Host-elements})$, where $E_{\text{tot}}(\text{Host-elements})$ represents the total energy of the standard state of the element constructing the host, eq 1 becomes the formation energy (E_f) of the layered intercalation compounds. A negative E_f value suggests that the reaction may proceed from the standard state of elements. In addition to E_{int} , E_f is also shown in the Supporting Information.

3. RESULTS

The objective of this study is to establish a new index for the stability of layered intercalation compounds. Considering the intercalant as the complex center and the host as the ligand, layered intercalation compounds are similar to complexes. We explored the possibility of applying the discussion on the stability of complex compounds. Various quantitative formulas, including the HSAB principle, have been proposed for the determination of the stability of complex compounds.^{68–70} Among them, Xu et al. reported a highly quantitative regression equation, eq 2, for the reaction energy of complex compounds⁷¹

$$2.303RT \log K_{\text{ML}} = \alpha_{\text{ML}}^* \Delta G_{\text{f},\text{M}^{n+}}^{\circ} + \beta_{\text{ML}}^* r_{\text{M}^{n+}} + \gamma_{\text{ML}}^* \Delta G_{\text{s},\text{M}^{n+}}^{\circ} - \delta_{\text{ML}}^* \quad (2)$$

where R is the gas constant, T is the temperature, K_{ML} represents the stability constants of the metal complex ML, $\Delta G_{\text{f},\text{M}^{n+}}^{\circ}$ is the standard Gibbs free energy of formation of M^{n+} , $r_{\text{M}^{n+}}$ is the ionic radius of M^{n+} , $\Delta G_{\text{s},\text{M}^{n+}}^{\circ}$ is the standard Gibbs free energy of dissolution of the aqueous ion M^{n+} , and α_{ML}^* , β_{ML}^* , γ_{ML}^* , and δ_{ML}^* are ligand-specific coefficients. In this equation, $2.303 RT \log K_{\text{ML}}$ represents the negative value of the reaction energy of the metal complex ML ($-\Delta G_{\text{r},\text{ML}}^{\circ}$), represented by the chemical equation $\text{M} + \text{L} \rightarrow \text{ML}$. It was proposed that $\alpha_{\text{ML}}^* \Delta G_{\text{f},\text{M}^{n+}}^{\circ}$ represents metal–ligand HSAB interactions, $\beta_{\text{ML}}^* r_{\text{M}^{n+}}$ represents ionic size effects, and $\Delta G_{\text{f},\text{M}^{n+}}^{\circ}$ is the “natural indices for the chemical hardness/softness”, referred to as “acid softness”. As a similar approach, limited to divalent cations, D.A. Sverjensky et al. reported that the energy of formation of inorganic crystalline solid substances can be described by the following linear regression eq 3⁷²

$$\Delta G_{\text{f},\text{M},\text{X}}^{\circ} = \alpha_{\text{M},\text{X}} \Delta G_{\text{n},\text{M}^{2+}}^{\circ} + \beta_{\text{M},\text{X}} r_{\text{M}^{2+}} + b_{\text{M},\text{X}} \quad (3)$$

where $\Delta G_{\text{f},\text{M},\text{X}}^{\circ}$ is the standard Gibbs free energy of formation for crystalline solids, $\Delta G_{\text{n},\text{M}^{2+}}^{\circ}$ is the nondissolved component of the standard Gibbs free energy of formation of M^{2+} ($\Delta G_{\text{n},\text{M}^{2+}}^{\circ} = \Delta G_{\text{f},\text{M}^{2+}}^{\circ} - \Delta G_{\text{s},\text{M}^{2+}}^{\circ}$), and $\alpha_{\text{M},\text{X}}$, $\beta_{\text{M},\text{X}}$, and $b_{\text{M},\text{X}}$ are regression coefficients specific to crystalline solids.

Based on these regression equations, we considered the intercalation energy E_{int} . As a result, we developed eq 4 as a new regression equation that incorporates HSAB-like interactions and size effects

$$E_{\text{int}} = \alpha_{\text{M-Host}} \Delta G_{\text{f},\text{M}^{n+}}^{\circ} + \frac{\beta_{\text{M-Host}}}{r_{\text{M}^{n+}}} + \gamma_{\text{M-Host}} \quad (4)$$

where $\Delta G_{\text{f},\text{M}^{n+}}^{\circ}$ and $r_{\text{M}^{n+}}$ are the standard Gibbs free energy of the M^{n+} ion and the ionic radii of the M^{n+} ion including positive and negative for n , respectively, and $\alpha_{\text{M-Host}}$, $\beta_{\text{M-Host}}$, and $\gamma_{\text{M-Host}}$ are the regression coefficients specific to the layered intercalation compounds with the same host and stacking structure obtained as a result of the screening in Figure 3. These values are determined for each of them.

To apply this equation, it is necessary to consider the combination of an anion-like (base-like) host for cationic intercalants and a cation-like (acid-like) host for anionic intercalants. Therefore, we classified the hosts according to the electronegativity of their constituent elements as follows: graphite in Figure 1(a) is classified as both acid-like and base-like, i.e., an amphoteric host; hosts in Figure 1(b–e), where the elements coordinating to the intercalant are highly electronegative, are classified as base-like hosts; and hosts in Figure 1(f,g), where the opposite configuration of Figure 1(b–e) is observed, are classified as acid-like hosts. We then performed host-specific regressions for the 41 cation intercalants with 169 base-like hosts and 7 anion intercalants with 24 acid-like hosts, resulting in a total of 193 regressions using 7097 data.

To confirm the validity of our regression model, the values of the adjusted coefficient of determination (Adj. R^2) for each variable combination and the sorted p -values calculated in the F-statistic test are shown in Figure 4(a,b). The regression results of the previously proposed model with eqs 2 and 3 were also compared.

It is evident that eq 4 demonstrates the best performance in terms of both Adj. R^2 and p -value. Particularly noteworthy is the p -value, where only eq 4 satisfies the criterion of p -value < 0.05 , signifying a significance level exceeding 95%, in all regressions. Its regression performance is higher than that of eq 2, which involves a regression using three variables. This superiority underscores the effectiveness of incorporating $1/r_{\text{M}^{n+}}$ as the Coulomb energy term.

Figure 4(c–f) illustrates the regression results of eq 4 with different accuracies and hosts, specifically, (A) the regression with the highest Adj. R^2 , (B) the regression with the highest Adj. R^2 in the base-like host, (C) the regression with medium Adj. R^2 , and (D) the regression with the lowest Adj. R^2 , indicated by arrows in Figure 4 (a). Even in the regression result with the lowest Adj. R^2 , the mean absolute error (MAE) is not considerably large as shown in Figure 4 (f). It appears that the small Adj. R^2 is due to the narrower energy range of the E_{int} distribution. This indicates that the performance of regression using eq 4 can capture the overall trend of stability even in the worst case.

All regression results for each of the 6929 data of cation intercalants and base-like hosts and 168 data of anions and acid-like hosts are presented in Figure 5(a,b), respectively. Both plots display the R^2 and MAE for the entire model calculated from all predicted values in eq 4, confirming the validity of the regression equation with a high linearity. In other words, in layered intercalation compounds, as in complex compounds, the compatibility between the host and intercalant can be understood by considering HSAB interactions and size effects (coulombic interactions).

For comparison, the same plot for eqs 2 and 3 is provided in Figures S7 and S8, respectively. The values of $\alpha_{\text{M-Host}}$, $\beta_{\text{M-Host}}$

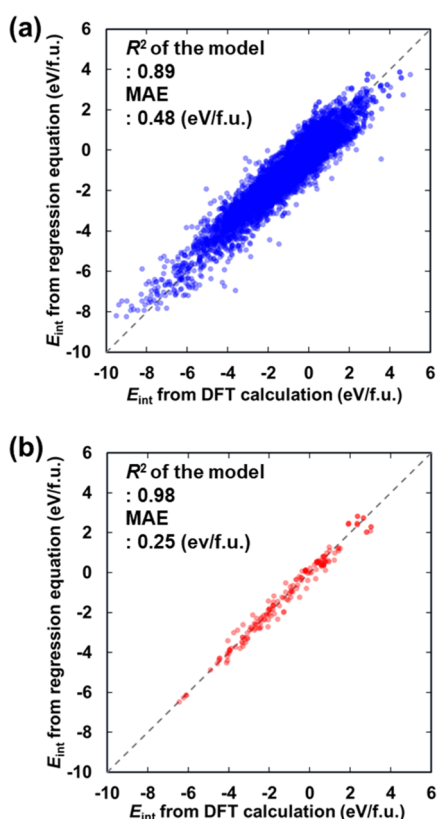


Figure 5. All results of the liner regressions by eq 4. (a) Cation intercalants and base-like hosts. (b) Anion intercalants and acid-like hosts.

and $\gamma_{M\text{-Host}}$ for each layered intercalation compound with the same host and stacking, along with the substances reported for each of them, are listed in the [Supporting Information](#).

4. DISCUSSION

As described above, regression results were obtained using eq 2 proposed by Xu et al. for complexes, eq 3 proposed by Sverhebsky et al. for inorganic crystals of divalent cations, and eq 4 proposed by us based on them. It is evident that eq 4 exhibits the best regression performance for the 7,097 layered intercalation compounds calculated in this study. We then

discuss the physical meaning of the optimal regression result in eq 4.

Based on previous studies, the first term $\alpha_{M\text{-Host}} \Delta G_{f,M}^{\circ}$ represents the HSAB-like interaction as in eq 2, while the second term $\beta_{M\text{-Host}} / r_M^n$ represents the size effect, distinct from eqs 2 and 3. Since this term involves the inverse of the ionic radius, it is considered to incorporate coulombic energy. These terms can be interpreted as the energy change due to electron transfer and electrostatic energy due to coulombic force. In this context, the regression coefficients $\alpha_{M\text{-Host}}$, $\beta_{M\text{-Host}}$ and $\gamma_{M\text{-Host}}$ can be considered the HSAB quantitative index for the host, the size effect quantitative index for the host, and the correction constant unique to each host, respectively.

To explore the relationship between these coefficients and regression eq 4 and to obtain a physical insight into the factors determining the stability of layered intercalation compounds, we attempted a decomposition of the intercalation process and energy, as illustrated in Figure 6.

$E_{\text{decohesion}, M}$ is the decohesion energy of the intercalant M from the standard state, $E_{\text{binding}, \text{Host}}$ is the binding energy of the layered structure host, $E_{\text{electron transfer}}$ is the electron (ne^- , n including positive and negative) transfer energy from the intercalant to the host, $E_{\text{binding}, M\text{-Host}}$ is the binding energy of the M-Host, and $E_{\text{straining}, \text{Host}}$ is the strain energy of the Host.

These decomposed energy components can be classified into three groups by colors: blue; M decohesion and electronic interaction, red; electrostatic Coulomb energy, and green; M-Host-dependent values, and they correspond to $\alpha_{M\text{-Host}} \Delta G_{f,M}^{\circ}$, $\beta_{M\text{-Host}} / r_M^n$, and $\gamma_{M\text{-Host}}$ in eq 4, respectively, as shown in Figure 6.

For example, the combination of the decohesion process of standard M and charge transfer process is analogous to the process by which M in the standard state ionized to form (hydrated) ions; it is reasonable that $E_{\text{decohesion}} + E_{\text{electron transfer}}$ correlates with $\Delta G_{f,M}^{\circ}$, as the blue part in the Figure 6, which represents the standard production energy of hydrated ions. In the same manner, second and third terms in eq 4 can be attributed to the decomposition process as shown in Figure 6, red and green parts, indicating that eq 4 and the terms are physically reasonable.

On the other hand, to predict the stability of the layered intercalation compounds solely from the intercalant–host

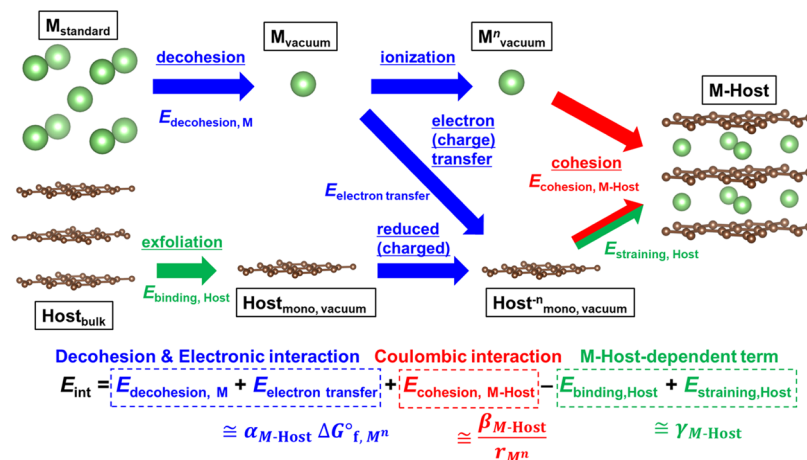


Figure 6. Decomposition of the intercalation process of a layered intercalation compound (M-Host) into distinct steps, accompanied by energy considerations and its presumed correlation with eq 4.

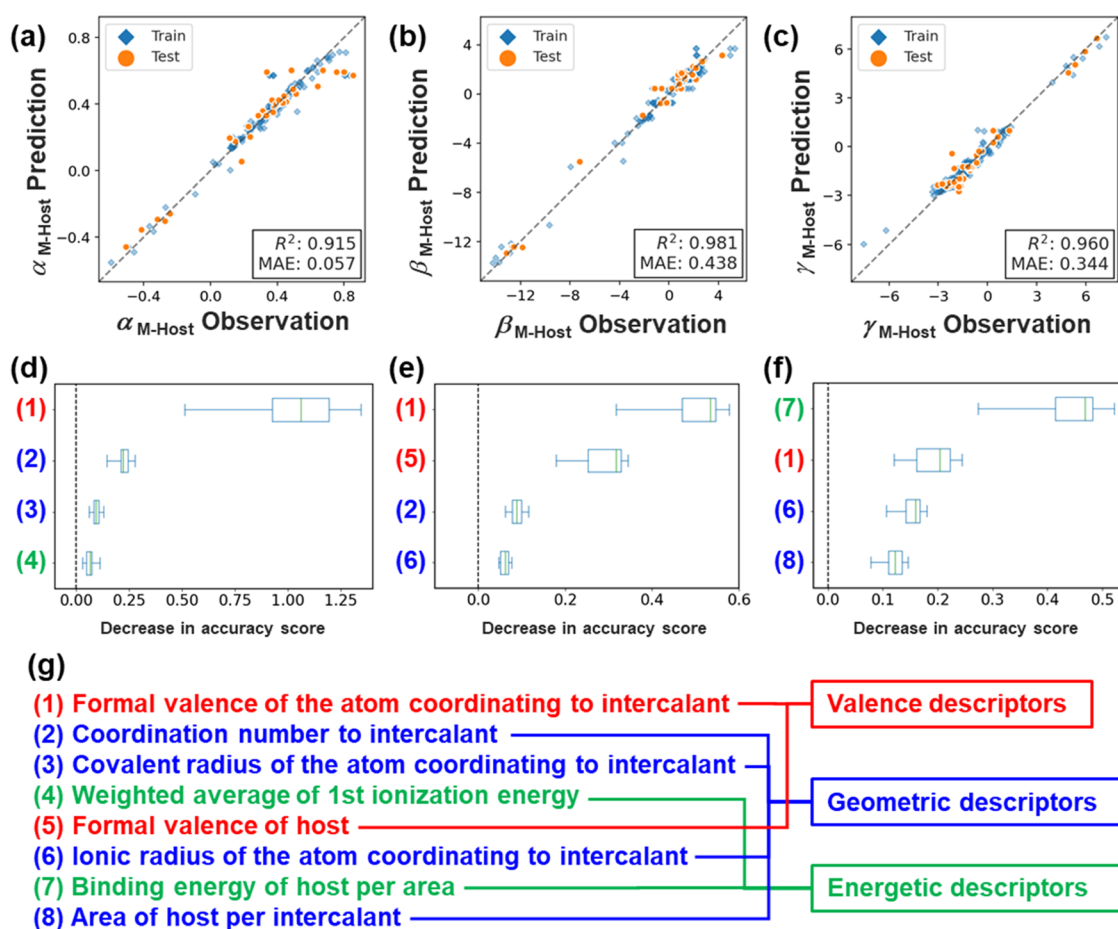


Figure 7. Results of the random forest regression. Correlation of the observed and predicted values of (a) $\alpha_{M\text{-Host}}$, (b) $\beta_{M\text{-Host}}$, and (c) $\gamma_{M\text{-Host}}$. The descriptor numbers of random forest regression and the results of permutation importance analysis for (d) $\alpha_{M\text{-Host}}$ prediction, (e) $\beta_{M\text{-Host}}$ prediction, and (f) $\gamma_{M\text{-Host}}$ prediction. (g) Detailed list of each descriptor.

combination before simulation and experimentation, determination of $\alpha_{M\text{-Host}}$, $\beta_{M\text{-Host}}$, and $\gamma_{M\text{-Host}}$ is necessary. These values are the host-dependent factors, and we investigated whether $\alpha_{M\text{-Host}}$, $\beta_{M\text{-Host}}$, and $\gamma_{M\text{-Host}}$ can be predicted from the compositional and physical properties of the host.

We examined regression by random forest regression,⁷³ a machine learning algorithm that predicts an objective variable while checking the importance of descriptors, using the scikit-learn library.⁷⁴ As a result of examining descriptors for various hosts, we succeeded in predicting them using four descriptors for each regression (eight descriptors in total). Figure 7(a–c) shows the regression results for $\alpha_{M\text{-Host}}$, $\beta_{M\text{-Host}}$, and $\gamma_{M\text{-Host}}$ respectively. Figure 7(d–f) shows the numbers of each descriptor used for prediction and the results of the permutation importance analysis. Figure 7(g) shows the details of each descriptor number. All data are split into 80% train data and 20% test data, and a random forest model trained on the train data is used to validate against the test set. Detailed condition for the random forest regression and the values of the descriptors are described in the Supporting Information.⁷⁵

In addition, the generalization performance of each model was evaluated by fivefold cross-validation, and the results are shown in Table 1. While there are some variations in R^2 for $\alpha_{M\text{-Host}}$ and $\gamma_{M\text{-Host}}$, the generalization performance is good for 193 sets of regression coefficients.

Looking at the permutation importance of each model, it can be seen that the value of (1) formal valence of the atom

Table 1. Results of Fivefold Cross-Validation

target		1	2	3	4	5	mean
$\alpha_{M\text{-Host}}$	test R^2	0.90	0.66	0.79	0.88	0.63	0.77
	train R^2	0.93	0.94	0.93	0.94	0.95	0.94
$\beta_{M\text{-Host}}$	test R^2	0.93	0.87	0.94	0.93	0.95	0.92
	train R^2	0.96	0.98	0.98	0.97	0.98	0.97
$\gamma_{M\text{-Host}}$	test R^2	0.96	0.84	0.88	0.59	0.84	0.83
	train R^2	0.96	0.97	0.97	0.98	0.97	0.97

coordinating to the intercalant is the most important descriptor. This value is considered to contain the basic information about whether the host is acid-like or base-like, and since it directly contacts the intercalant, it is reasonable to say that it greatly affects the compatibility with the intercalant. For $\beta_{M\text{-Host}}$, (5) the formal valence of the host is also important, which is consistent to the meanings of the second term of eq 4, the coulombic interaction. For $\alpha_{M\text{-Host}}$ and $\beta_{M\text{-Host}}$, the contribution of (2) the coordination number to intercalants tends to be high. This reflects the geometric information around the intercalant. Actually, other important factors for $\alpha_{M\text{-Host}}$ and $\beta_{M\text{-Host}}$ (3) and (6), are commonly related to the radius of the coordinating atoms. The last important descriptor for $\alpha_{M\text{-Host}}$ is (4) weighted average of first ionization energies of the elements constituting the host, which is considered to incorporate the effect of electron transfer as shown in Figure 6. As for $\gamma_{M\text{-Host}}$, (7) binding energy of the

host, (6) ionic radius of the coordination atom, and (8) area per intercalant are the important descriptors, which also show that the model successfully incorporates the effects of $E_{\text{binding, Host}}$ and $E_{\text{straining, Host}}$ as shown in Figure 6.

Finally, the comparison of E_{int} calculated by eq 4 with the predicted $\alpha_{\text{M-Host}}$, $\beta_{\text{M-Host}}$, and $\gamma_{\text{M-Host}}$ for the compounds in the test data of Figure 7 and that by DFT is shown in Figure 8. Although R^2 is not high (0.68), eq 4 and parameters have the potential to predict the E_{int} with the accuracy of 0.75 eV/f.u.

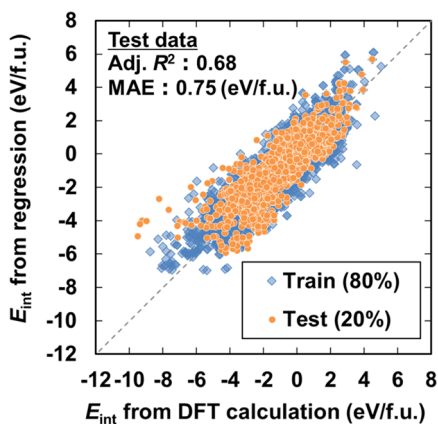


Figure 8. Comparison of E_{int} calculated by DFT and predicted by regression eq 4 with predicted regression coefficients from random forest regression.

We have also confirmed that E_{int} can be predicted by machine learning methods, although the physics cannot be interpreted as well as the regression model that we have developed. The results are shown in Figure S9 in the Supporting Information. Figure S9 (a) shows the results of random forest regression using two intercalant properties ($\Delta G_{\text{f},\text{M}}^{\circ}$ and r_{M^n}) and eight host properties (shown in Figure 7) as descriptors by random forest, and Figure S9 (b) shows the results of prediction using Crystal Graph Convolutional Neural Networks (CGCNN).⁷⁶ It can be seen that both methods can predict E_{int} with good accuracy. However, these models lack physical support and are not validated with respect to extrapolative application to unknown material systems. This stands in contrast to our regression model, which relies on a simple and physically reasonable formulation. Through this study, we succeeded in extracting the underlying physics to estimate the intercalation energy only from two intercalant properties and eight host-derived descriptors by random forest and regression equations without the first-principles calculations.

5. CONCLUSIONS

We constructed a database of layered intercalation compounds and successfully developed a regression equation to predict the intercalation energy of layered intercalation compounds based on two properties of the intercalant: $\Delta G_{\text{f},\text{M}}^{\circ}$ and the inverse of r_{M^n} . We investigated the coefficients for the equation, demonstrating their prediction using a machine learning approach. This enables the estimation of intercalation energy without first-principles calculations.

■ ASSOCIATED CONTENT

Supporting Information

The Supporting Information is available free of charge at <https://pubs.acs.org/doi/10.1021/acspchemau.3c00063>.

Structures of layered intercalation compounds, comparison of total energy in different energy convergence thresholds, results of regression in other models, prediction of E_{int} by the machine learning methods, comparison of the vdW correction methods, values of $\Delta G_{\text{f},\text{M}}^{\circ}$ and r_{M^n} of intercalant, and conditions of random forest regression (PDF)

Values of E_{int} and E_{f} of all layered intercalation compounds, Adj. R^2 , $\alpha_{\text{M-Host}}$, $\beta_{\text{M-Host}}$ and $\gamma_{\text{M-Host}}$ of each layered intercalation compounds with the same host and stacking, and value of descriptors for random forest regressions (XLSX)

■ AUTHOR INFORMATION

Corresponding Authors

Naoto Kawaguchi – Department of Materials Science and Engineering, The University of Tokyo, Tokyo 113-8656, Japan; orcid.org/0000-0002-8100-2643; Email: nkawa@iis.u-tokyo.ac.jp

Teruyasu Mizoguchi – Department of Materials Science and Engineering, The University of Tokyo, Tokyo 113-8656, Japan; Institute of Industrial Science, The University of Tokyo, Tokyo 153-8505, Japan; orcid.org/0000-0003-3712-7307; Email: teru@iis.u-tokyo.ac.jp

Author

Kiyou Shibata – Department of Materials Science and Engineering, The University of Tokyo, Tokyo 113-8656, Japan; Institute of Industrial Science, The University of Tokyo, Tokyo 153-8505, Japan; orcid.org/0000-0002-0639-5408

Complete contact information is available at: <https://pubs.acs.org/10.1021/acspchemau.3c00063>

Author Contributions

The article was written through contributions of all authors. All authors have given approval to the final version of the article. CRediT: **Naoto Kawaguchi** conceptualization, data curation, formal analysis, investigation, methodology, visualization, writing-original draft; **Kiyou Shibata** conceptualization, methodology, resources, supervision, writing-review & editing; **Teruyasu Mizoguchi** conceptualization, funding acquisition, methodology, project administration, resources, software, supervision, writing-review & editing.

Funding

This study was supported by the Ministry of Education, Culture, Sports, Science and Technology (MEXT) (grant no. 19H00818 and 19H05787) and the special fund (Tenkai) by the Institute of Industrial Science, the University of Tokyo.

Notes

The authors declare the following competing financial interest(s): The authors declare the following financial interests/personal relationships which may be considered as potential competing interests: Naoto Kawaguchi reports financial support was provided by Resonac Corporation.

ACKNOWLEDGMENTS

The authors thank Dr. Hiraku Ogino of the National Institute of Advanced Industrial Science and Technology for the discussions about applying the HSAB principle for crystalline inorganic materials. The authors also thank Prof. Shunsuke Yagi and Prof. Takanari Ouchi in the University of Tokyo for the discussions about the possibility of synthesis of the new layered intercalation compounds.

REFERENCES

- (1) Mizushima, K.; Jones, P. C.; Wiseman, P. J.; Goodenough, J. B. Li_xCoO_2 ($0 < x \leq 1$): A New Cathode Material for Batteries of High Energy Density. *Mater. Res. Bull.* **1980**, *15* (6), 783–789.
- (2) Yazami, R.; Touzain, Ph. A Reversible Graphite-Lithium Negative Electrode for Electrochemical Generators. *J. Power Sources* **1983**, *9* (3), 365–371.
- (3) Hannay, N. B.; Geballe, T. H.; Matthias, B. T.; Andres, K.; Schmidt, P.; MacNair, D. Superconductivity in Graphitic Compounds. *Phys. Rev. Lett.* **1965**, *14* (7), 225–226.
- (4) Hor, Y. S.; Williams, A. J.; Checkelsky, J. G.; Roushan, P.; Seo, J.; Xu, Q.; Zandbergen, H. W.; Yazdani, A.; Ong, N. P.; Cava, R. J. Superconductivity in $\text{Cu}_x\text{Bi}_2\text{Se}_3$ and Its Implications for Pairing in the Undoped Topological Insulator. *Phys. Rev. Lett.* **2010**, *104* (5), No. 057001.
- (5) Rendenbach, B.; Hohl, T.; Harm, S.; Hoch, C.; Johrendt, D. Electrochemical Synthesis and Crystal Structure of the Organic Ion Intercalated Superconductor $(\text{TMA})_{0.5}\text{Fe}_2\text{Se}_2$ with $T_c = 43$ K. *J. Am. Chem. Soc.* **2021**, *143* (8), 3043–3048.
- (6) Kong, Z.; Kaminsky, C. J.; Groschner, C. K.; Murphy, R. A.; Yu, Y.; Husremović, S.; Xie, L. S.; Erodić, M. P.; Kim, R. S.; Yano, J.; Bediako, D. K. Near Room-Temperature Intrinsic Exchange Bias in an Fe Intercalated ZrSe_2 Spin Glass. *J. Am. Chem. Soc.* **2023**, *145* (36), 20041–20052.
- (7) Inoshita, T.; Hirayama, M.; Hamada, N.; Hosono, H.; Murakami, S. Topological Semimetal Phases Manifested in Transition Metal Dichalcogenides Intercalated with 3d Metals. *Phys. Rev. B* **2019**, *100* (12), No. 121112.
- (8) Papaderakis, A. A.; Ejigu, A.; Yang, J.; Elgendy, A.; Radha, B.; Keerthi, A.; Juel, A.; Dryfe, R. A. W. Anion Intercalation into Graphite Drives Surface Wetting. *J. Am. Chem. Soc.* **2023**, *145* (14), 8007–8020.
- (9) Wang, N.; Tang, H.; Shi, M.; Zhang, H.; Zhuo, W.; Liu, D.; Meng, F.; Ma, L.; Ying, J.; Zou, L.; Sun, Z.; Chen, X. Transition from Ferromagnetic Semiconductor to Ferromagnetic Metal with Enhanced Curie Temperature in $\text{Cr}_2\text{Ge}_2\text{Te}_6$ via Organic Ion Intercalation. *J. Am. Chem. Soc.* **2019**, *141* (43), 17166–17173.
- (10) Koski, K. J.; Wessells, C. D.; Reed, B. W.; Cha, J. J.; Kong, D.; Cui, Y. Chemical Intercalation of Zerovalent Metals into 2D Layered Bi_2Se_3 Nanoribbons. *J. Am. Chem. Soc.* **2012**, *134* (33), 13773–13779.
- (11) Cahen, S.; Lagrange, P.; Maréché, J.-F.; Hérol, C. Analogies and Differences between Calcium-Based and Europium-Based Graphite Intercalation Compounds. *C. R. Chim.* **2013**, *16* (4), 385–390.
- (12) Bolmont, M.; Cahen, S.; Fauchard, M.; Guillot, R.; Medjahdi, G.; Berger, P.; Lamura, G.; Lagrange, P.; Hérol, C. LiCl-KCl Eutectic Molten Salt as an Original and Efficient Medium to Intercalate Metals into Graphite: Case of Europium. *Carbon N Y* **2018**, *133*, 379–383.
- (13) Zhao, X.; Song, P.; Wang, C.; Riis-Jensen, A. C.; Fu, W.; Deng, Y.; Wan, D.; Kang, L.; Ning, S.; Dan, J.; Venkatesan, T.; Liu, Z.; Zhou, W.; Thygesen, K. S.; Luo, X.; Pennycook, S. J.; Loh, K. P. Engineering Covalently Bonded 2D Layered Materials by Self-Intercalation. *Nature* **2020**, *581* (7807), 171–177.
- (14) Jain, A.; Hautier, G.; Moore, C. J.; Ping Ong, S.; Fischer, C. C.; Mueller, T.; Persson, K. A.; Ceder, G. A High-Throughput Infrastructure for Density Functional Theory Calculations. *Comput. Mater. Sci.* **2011**, *50* (8), 2295–2310.
- (15) Nishijima, M.; Ootani, T.; Kamimura, Y.; Sueki, T.; Esaki, S.; Murai, S.; Fujita, K.; Tanaka, K.; Ohira, K.; Koyama, Y.; Tanaka, I. Accelerated Discovery of Cathode Materials with Prolonged Cycle Life for Lithium-Ion Battery. *Nat. Commun.* **2014**, *5* (1), 4553.
- (16) Ong, S. P.; Mo, Y.; Richards, W. D.; Miara, L.; Lee, H. S.; Ceder, G. Phase Stability, Electrochemical Stability and Ionic Conductivity of the $\text{Li}_{10\pm 1}\text{MP}_2\text{X}_{12}$ ($\text{M} = \text{Ge}, \text{Si}, \text{Sn}, \text{Al}$ or P , and $\text{X} = \text{O}, \text{S}$ or Se) Family of Superionic Conductors. *Energy Environ. Sci.* **2013**, *6* (1), 148–156.
- (17) Hinuma, Y.; Hatakeyama, T.; Kumagai, Y.; Burton, L. A.; Sato, H.; Muraba, Y.; Iimura, S.; Hiramatsu, H.; Tanaka, I.; Hosono, H.; Oba, F. Discovery of Earth-Abundant Nitride Semiconductors by Computational Screening and High-Pressure Synthesis. *Nat. Commun.* **2016**, *7*, No. 11962, DOI: 10.1038/ncomms11962.
- (18) Hohenberg, P.; Kohn, W. Inhomogeneous Electron Gas. *Phys. Rev.* **1964**, *136* (3B), B864–B871.
- (19) Kohn, W.; Sham, L. J. Self-Consistent Equations Including Exchange and Correlation Effects. *Phys. Rev.* **1965**, *140* (4A), A1133–A1138.
- (20) Jain, A.; Ong, S. P.; Hautier, G.; Chen, W.; Richards, W. D.; Dacek, S.; Cholia, S.; Gunter, D.; Skinner, D.; Ceder, G.; Persson, K. A. Commentary: The Materials Project: A Materials Genome Approach to Accelerating Materials Innovation. *APL Mater.* **2013**, *1* (1), No. 011002.
- (21) Saal, J. E.; Kirklín, S.; Aykol, M.; Meredig, B.; Wolverton, C. Materials Design and Discovery with High-Throughput Density Functional Theory: The Open Quantum Materials Database (OQMD). *JOM* **2013**, *65* (11), 1501–1509.
- (22) Kirklín, S.; Saal, J. E.; Meredig, B.; Thompson, A.; Doak, J. W.; Aykol, M.; Rühl, S.; Wolverton, C. The Open Quantum Materials Database (OQMD): Assessing the Accuracy of DFT Formation Energies. *NPJ. Comput. Mater.* **2015**, *1* (1), No. 15010.
- (23) Nitta, N.; Wu, F.; Lee, J. T.; Yushin, G. Li-Ion Battery Materials: Present and Future. *Mater. Today* **2015**, *18* (5), 252–264.
- (24) Obrovac, M. N.; Chevriér, V. L. Alloy Negative Electrodes for Li-Ion Batteries. *Chem. Rev.* **2014**, *114* (23), 11444–11502.
- (25) Mounet, N.; Gibertini, M.; Schwaller, P.; Campi, D.; Merkys, A.; Marrazzo, A.; Sohier, T.; Castelli, I. E.; Cepellotti, A.; Pizzi, G.; Marzari, N. Two-Dimensional Materials from High-Throughput Computational Exfoliation of Experimentally Known Compounds. *Nat. Nanotechnol.* **2018**, *13* (3), 246–252.
- (26) Hastrup, S.; Strange, M.; Pandey, M.; Deilmann, T.; Schmidt, P. S.; Hinsche, N. F.; Gjerding, M. N.; Torelli, D.; Larsen, P. M.; Riis-Jensen, A. C.; Gath, J.; Jacobsen, K. W.; Jørgen Mortensen, J.; Olsen, T.; Thygesen, K. S. The Computational 2D Materials Database: High-Throughput Modeling and Discovery of Atomically Thin Crystals. *2d Mater.* **2018**, *5* (4), No. 042002.
- (27) Zhou, J.; Shen, L.; Costa, M. D.; Persson, K. A.; Ong, S. P.; Huck, P.; Lu, Y.; Ma, X.; Chen, Y.; Tang, H.; Feng, Y. P. 2DMatPedia, an Open Computational Database of Two-Dimensional Materials from Top-down and Bottom-up Approaches. *Sci. Data* **2019**, *6* (1), 86.
- (28) Emery, A. A.; Wolverton, C. High-Throughput DFT Calculations of Formation Energy, Stability and Oxygen Vacancy Formation Energy of ABO_3 Perovskites. *Sci. Data* **2017**, *4*, 170153.
- (29) Scheidgen, M.; Himanen, L.; Ladines, A. N.; Sikter, D.; Nakhaee, M.; Fekete, Á.; Chang, T.; Golparvar, A.; Márquez, J. A.; Brockhauser, S.; Brückner, S.; Ghiringhelli, L. M.; Dietrich, F.; Lehmborg, D.; Denell, T.; Albino, A.; Näsström, H.; Shabih, S.; Dobener, F.; Kühbach, M.; Mozumdar, R.; Rudzinski, J. F.; Daelman, N.; Pizarro, J. M.; Kuban, M.; Salazar, C.; Ondračka, P.; Bungartz, H.-J.; Draxl, C. NOMAD: A Distributed Web-Based Platform for Managing Materials Science Research Data. *J. Open Source Software* **2023**, *8* (90), 5388.
- (30) Clark, S. J.; Segall, M. D.; Pickard, C. J.; Hasnip, P. J.; Probert, M. I. J.; Refson, K.; Payne, M. C. First Principles Methods Using CASTEP. *Z. Kristallogr. Cryst. Mater.* **2005**, *220* (5–6), S67–S70.
- (31) Kresse, G.; Hafner, J. *Ab Initio* Molecular Dynamics for Liquid Metals. *Phys. Rev. B* **1993**, *47* (1), S58–S61.

- (32) Kresse, G.; Hafner, J. *Ab Initio* Molecular-Dynamics Simulation of the Liquid-Metal–Amorphous-Semiconductor Transition in Germanium. *Phys. Rev. B* **1994**, *49* (20), 14251–14269.
- (33) Kresse, G.; Furthmüller, J. Efficiency of Ab-Initio Total Energy Calculations for Metals and Semiconductors Using a Plane-Wave Basis Set. *Comput. Mater. Sci.* **1996**, *6* (1), 15–50.
- (34) Kresse, G.; Furthmüller, J. Efficient Iterative Schemes for *Ab Initio* Total-Energy Calculations Using a Plane-Wave Basis Set. *Phys. Rev. B* **1996**, *54* (16), 11169–11186.
- (35) Kresse, G.; Joubert, D. From Ultrasoft Pseudopotentials to the Projector Augmented-Wave Method. *Phys. Rev. B* **1999**, *59* (3), 1758–1775.
- (36) Giannozzi, P.; Baroni, S.; Bonini, N.; Calandra, M.; Car, R.; Cavazzoni, C.; Ceresoli, D.; Chiarotti, G. L.; Cococcioni, M.; Dabo, I.; Dal Corso, A.; de Gironcoli, S.; Fabris, S.; Fratesi, G.; Gebauer, R.; Gerstmann, U.; Gougousis, C.; Kokalj, A.; Lazzeri, M.; Martin-Samos, L.; Marzari, N.; Mauri, F.; Mazzarello, R.; Paolini, S.; Pasquarello, A.; Paulatto, L.; Sbraccia, C.; Scandolo, S.; Sclauzero, G.; Seitsonen, A. P.; Smogunov, A.; Umari, P.; Wentzcovitch, R. M. QUANTUM ESPRESSO: A Modular and Open-Source Software Project for Quantum Simulations of Materials. *J. Phys.: Condens. Matter* **2009**, *21* (39), No. 395502.
- (37) Giannozzi, P.; Andreussi, O.; Brumme, T.; Bunau, O.; Nardelli, M. B.; Calandra, M.; Car, R.; Cavazzoni, C.; Ceresoli, D.; Cococcioni, M.; Colonna, N.; Carnimeo, I.; Dal Corso, A.; De Gironcoli, S.; Delugas, P.; Distasio, R. A.; Ferretti, A.; Floris, A.; Fratesi, G.; Fugallo, G.; Gebauer, R.; Gerstmann, U.; Giustino, F.; Gorni, T.; Jia, J.; Kawamura, M.; Ko, H. Y.; Kokalj, A.; Küçükbenli, E.; Lazzeri, M.; Marsili, M.; Marzari, N.; Mauri, F.; Nguyen, N. L.; Nguyen, H. V.; Otero-De-La-Roza, A.; Paulatto, L.; Poncé, S.; Rocca, D.; Sabatini, R.; Santra, B.; Schlipf, M.; Seitsonen, A. P.; Smogunov, A.; Timrov, I.; Thonhauser, T.; Umari, P.; Vast, N.; Wu, X.; Baroni, S. Advanced Capabilities for Materials Modelling with Quantum ESPRESSO. *J. Phys.: Condens. Matter* **2017**, *29* (46), No. 465901, DOI: 10.1088/1361-648X/aa8f79.
- (38) Rupp, M.; Tkatchenko, A.; Müller, K.-R.; von Lilienfeld, O. A. Fast and Accurate Modeling of Molecular Atomization Energies with Machine Learning. *Phys. Rev. Lett.* **2012**, *108* (5), No. 058301.
- (39) Pham, T.-L.; Nguyen, N.-D.; Nguyen, V.-D.; Kino, H.; Miyake, T.; Dam, H.-C. Learning Structure-Property Relationship in Crystalline Materials: A Study of Lanthanide–Transition Metal Alloys. *J. Chem. Phys.* **2018**, *148* (20), No. 204106.
- (40) Lam Pham, T.; Kino, H.; Terakura, K.; Miyake, T.; Tsuda, K.; Takigawa, I.; Chi Dam, H. Machine Learning Reveals Orbital Interaction in Materials. *Sci. Technol. Adv. Mater.* **2017**, *18* (1), 756–765.
- (41) Zhou, J.; Lin, Z.; Ren, H.; Duan, X.; Shakir, I.; Huang, Y.; Duan, X. Layered Intercalation Materials. *Adv. Mater.* **2021**, *33* (25), No. 2004557, DOI: 10.1002/adma.202004557.
- (42) Liu, X.-C.; Zhao, S.; Sun, X.; Deng, L.; Zou, X.; Hu, Y.; Wang, Y.-X.; Chu, C.-W.; Li, J.; Wu, J.; Ke, F.-S.; Ajayan, P. M. Spontaneous Self-Intercalation of Copper Atoms into Transition Metal Dichalcogenides. *Sci. Adv.* **2020**, *6* (7), 4092–4106.
- (43) Kawaguchi, N.; Shibata, K.; Mizoguchi, T. Possible New Graphite Intercalation Compounds for Superconductors and Charge Density Wave Materials: Systematic Simulations with Various Intercalants Using a van Der Waals Density Functional Method. *J. Phys. Chem. C* **2023**, *127*, 9833.
- (44) Pearson, R. G. Hard and Soft Acids and Bases. *J. Am. Chem. Soc.* **1963**, *85* (22), 3533–3539.
- (45) Pearson, R. G. Acids and Bases. *Science* **1966**, *151* (3707), 172–177.
- (46) Parr, R. G.; Pearson, R. G. Absolute Hardness: Companion Parameter to Absolute Electronegativity. *J. Am. Chem. Soc.* **1983**, *105* (26), 7512–7516.
- (47) Kaya, C.; Kaya, S.; Banerjee, P. A Novel Lattice Energy Calculation Technique for Simple Inorganic Crystals. *Phys.: Condens. Matter* **2017**, *504*, 127–132.
- (48) Moriwake, H.; Kuwabara, A.; Fisher, C. A. J.; Ikuhara, Y. Why Is Sodium-Intercalated Graphite Unstable? *RSC Adv.* **2017**, *7* (58), 36550–36554.
- (49) Lenchuk, O.; Adelhelm, P.; Mollenhauer, D. New Insights into the Origin of Unstable Sodium Graphite Intercalation Compounds. *Phys. Chem. Chem. Phys.* **2019**, *21* (35), 19378–19390.
- (50) Allred, A. L.; Rochow, E. G. A Scale of Electronegativity Based on Electrostatic Force. *J. Inorg. Nucl. Chem.* **1958**, *5* (4), 264–268.
- (51) Momma, K.; Izumi, F. VESTA 3 for Three-Dimensional Visualization of Crystal, Volumetric and Morphology Data. *J. Appl. Crystallogr.* **2011**, *44* (6), 1272–1276.
- (52) Pourbaix, M. *Atlas of Electrochemical Equilibria in Aqueous Solutions*; NACE International Cebelcor: Brussel, 1974.
- (53) Shock, E. L.; Helgeson, H. C. Calculation of the Thermodynamic and Transport Properties of Aqueous Species at High Pressures and Temperatures: Correlation Algorithms for Ionic Species and Equation of State Predictions to 5 kb and 1000°C. *Geochim. Cosmochim. Acta* **1988**, *52* (8), 2009–2036.
- (54) Shock, E. L.; Sassani, D. C.; Willis, M.; Sverjensky, D. A. Inorganic Species in Geologic Fluids: Correlations among Standard Molal Thermodynamic Properties of Aqueous Ions and Hydroxide Complexes. *Geochim. Cosmochim. Acta* **1997**, *61* (5), 907–950.
- (55) Shannon, R. D. Revised Effective Ionic Radii and Systematic Studies of Interatomic Distances in Halides and Chalcogenides. *Acta Crystallogr., Sect. A* **1976**, *32* (5), 751–767.
- (56) Marcus, Y. Thermodynamics of Solvation of Ions. Part 5.—Gibbs Free Energy of Hydration at 298.15 K. *J. Chem. Soc., Faraday Trans.* **1991**, *87* (18), 2995–2999.
- (57) Blöchl, P. E. Projector Augmented-Wave Method. *Phys. Rev. B* **1994**, *50* (24), 17953–17979.
- (58) Dion, M.; Rydberg, H.; Schröder, E.; Langreth, D. C.; Lundqvist, B. I. Van Der Waals Density Functional for General Geometries. *Phys. Rev. Lett.* **2004**, *92* (24), No. 246401.
- (59) Lee, K.; Murray, E. D.; Kong, L.; Lundqvist, B. I.; Langreth, D. C. Higher-Accuracy van Der Waals Density Functional. *Phys. Rev. B* **2010**, *82* (8), No. 081101.
- (60) Klimeš, J.; Bowler, D. R.; Michaelides, A. Chemical Accuracy for the van Der Waals Density Functional. *J. Phys.: Condens. Matter* **2010**, *22* (2), No. 022201, DOI: 10.1088/0953-8984/22/2/022201.
- (61) Klimeš, J.; Bowler, D. R.; Michaelides, A. Van Der Waals Density Functionals Applied to Solids. *Phys. Rev. B* **2011**, *83* (19), No. 195131.
- (62) Hamada, I. Van Der Waals Density Functional Made Accurate. *Phys. Rev. B* **2014**, *89* (12), No. 121103.
- (63) Peng, H.; Yang, Z.-H.; Perdew, J. P.; Sun, J. Versatile van Der Waals Density Functional Based on a Meta-Generalized Gradient Approximation. *Phys. Rev. X* **2016**, *6* (4), No. 041005.
- (64) Román-Pérez, G.; Soler, J. M. Efficient Implementation of a van Der Waals Density Functional: Application to Double-Wall Carbon Nanotubes. *Phys. Rev. Lett.* **2009**, *103* (9), No. 096102.
- (65) Monkhorst, H. J.; Pack, J. D. Special Points for Brillouin-Zone Integrations. *Phys. Rev. B* **1976**, *13* (12), 5188–5192.
- (66) Blöchl, P. E.; Jepsen, O.; Andersen, O. K. Improved Tetrahedron Method for Brillouin-Zone Integrations. *Phys. Rev. B* **1994**, *49* (23), 16223–16233.
- (67) Aydinol, M. K.; Kohan, A. F.; Ceder, G.; Cho, K.; Joannopoulos, J. *Ab Initio* Study of Lithium Intercalation in Metal Oxides and Metal Dichalcogenides. *Phys. Rev. B* **1997**, *56* (3), 1354–1365.
- (68) Hudson, R. F.; Klopman, G. A General Perturbation Treatment of Chemical Reactivity. *Tetrahedron Lett.* **1967**, *8* (12), 1103–1108.
- (69) Drago, R. S.; Wayland, B. B. A Double-Scale Equation for Correlating Enthalpies of Lewis Acid-Base Interactions. *J. Am. Chem. Soc.* **1965**, *87* (16), 3571–3577.
- (70) Hancock, R. D.; Martell, A. E. Lewis Acid–Base Behavior in Aqueous Solution: Some Implications for Metal Ions in Biology. *Adv. Inorg. Chem.* **1995**, *42*, 89–146.

(71) Xu, H.; Xu, D. C.; Wang, Y. Natural Indices for the Chemical Hardness/Softness of Metal Cations and Ligands. *ACS Omega* **2017**, *2* (10), 7185–7193.

(72) Sverjensky, D. A.; Molling, P. A. A Linear Free Energy Relationship for Crystalline Solids and Aqueous Ions. *Nature* **1992**, *356*, 231–234.

(73) Tin Kam Ho Random Decision Forests. In *Proceedings of 3rd International Conference on Document Analysis and Recognition*; IEEE Comput. Soc. Press, 1995; Vol. 1, pp 278–282 DOI: [10.1109/ICDAR.1995.598994](https://doi.org/10.1109/ICDAR.1995.598994).

(74) Pedregosa, F.; Varoquaux, G.; Gramfort, A.; Michel, V.; Thirion, B.; Grisel, O.; Blondel, M.; Peter, P.; Weiss, R.; Dubourg, V.; Vanderplas, J.; Passos, A.; Cournapeau, D.; Brucher, M.; Perrot, M.; Duchesnay, E. Scikit-Learn: Machine Learning in Python. *J. Mach Learn. Res.* **2011**, *12* (85), 2825–2830. scikit-learn (accessed 2024–02–08).

(75) Ouyang, R. Exploiting Ionic Radii for Rational Design of Halide Perovskites. *Chem. Mater.* **2020**, *32* (1), 595–604.

(76) Xie, T.; Grossman, J. C. Crystal Graph Convolutional Neural Networks for an Accurate and Interpretable Prediction of Material Properties. *Phys. Rev. Lett.* **2018**, *120* (14), No. 145301.